Available online at www.sciencedirect.com
ScienceDirect
Polymer 47 (2006) 7980–7987
polymer
www.elsevier.com/locate/polymer

Cascade analysis of mixed gels of xanthan and locust bean gum

Ching-Feng Mao [a,*], Syang-Peng Rwei [b]

[a] Department of Chemical and Material Engineering, Southern Taiwan University of Technology, No. 1, Nan-Tai St., YungKung City, Tainan 710, Taiwan, ROC
[b] Institute of Organic/Polymeric Materials, National Taipei University of Technology, No. 1, Sec. 3, Chung-Hsiao E. Rd., Taipei 106, Taiwan, ROC

Received 29 May 2006; received in revised form 21 August 2006; accepted 15 September 2006
Available online 10 October 2006

Abstract

The gel properties of xanthan (XG)–locust bean gum (LBG) mixtures were investigated. The concentration and temperature dependence of gel modulus, as well as the composition dependence of critical gelling concentration, were analyzed using a cascade model. The number of cross-linking sites per molecule for XG and LBG, f_{XG} and f_{LBG}, is determined by fitting experimental data to the model. The values of $f_{XG} = 100$ and $f_{LBG} = 1000$, obtained from the concentration dependence of gel modulus, imply that a cross-link is formed in every 10 repeating units along the XG backbone and the cross-linking site in LBG is composed of segments with more than three consecutive unsubstituted mannose residues. An anomalously high value of f_{XG} is obtained from the temperature dependence of gel modulus, probably due to the existence of a secondary mechanism during the rheological meltdown process. The cascade analysis of the composition dependence of critical gelling concentration results in values of $f_{XG} = 30$ and $f_{LBG} = 5$. These values reflect that the critical gelling concentration measurement probes only the cross-links formed via long segments of XG and LBG.
© 2006 Elsevier Ltd. All rights reserved.

Keywords: Cascade model; Mixed gels; Gel modulus

1. Introduction

The synergistic interaction between two different polysaccharides in solutions often leads to an increase in solution viscosity or the formation of gels [1]. This subject has attracted the interest of many researchers during the last two decades due to its effectiveness in reducing production costs and enhancing rheological properties. Among these multi-component systems, probably the most intensively studied is the xanthan/galactomannan mixed gel [2–5], where the gel network is formed via the synergistic interaction of xanthan with galactomannan.

Xanthan gum (XG) is a natural polysaccharide produced by the bacterium *Xanthomonas campestris*. The primary structure of xanthan consists of a cellulose backbone, substituted alternately with a trisaccharide side chain [6,7]. The side chain is composed of a glucuronic acid residue between two mannose residues, where the terminal residue may contain pyruvic acid and the inner residue is normally acetylated. It is known that xanthan in aqueous solutions adopts a rigid, ordered conformation as a double-stranded helix with a persistence length of about 150 nm [8,9]. On heating, it undergoes an order–disorder transition from helix to random coil [10,11]. Factors such as ionic strength [10], content of pyruvate and acetate substituents [12] also affect the stability of the ordered conformation. At moderate concentrations xanthan undergoes self-association to form a ''weak gel'' [13], which flows under a steady stress. When mixed with certain polysaccharides such as galactomannan and glucomannan, xanthan forms a true gel [3].

Galactomannan is a seed polysaccharide consisting of a mannan backbone, attached randomly with a single galactose side chain [14]. The physicochemical properties of galactomannan strongly depend on its galactose content. Unsubstituted mannan is completely insoluble in water, whereas the solubility of galactomannan increases with increasing galactose content. Locust bean gum (LBG) and guar gum are two of the most widely used galactomannans. The former has a mannose to galactose ratio of 4:1 and is slightly soluble in cold water but dissolves when heated up to 80 °C [15]. The latter, on the other hand, has a mannose to galactose ratio of 2:1 and is more

* Corresponding author. Tel.: +886 2 27712171x2432; fax: +886 6 2425741.
E-mail address: cfmao@mail.stut.edu.tw (C.-F. Mao).

0032-3861/$ - see front matter © 2006 Elsevier Ltd. All rights reserved.
doi:10.1016/j.polymer.2006.09.032

soluble than LBG. The increase in solubility is attributed to the extensive hydration of the galactose-rich regions. LBG solutions are known to form a gel after freeze–thaw cycles [1,16]. The gel network is attributed to the interaction between unsubstituted mannan segments, which is promoted by the formation of a polymer-rich region during the freeze–thaw cycle.

The combination of XG and LBG is known to yield a strong synergistic gel. The cross-linking site of LBG has been suggested to be composed of consecutive unsubstituted mannan segments [17]. For xanthan, the interaction has been proposed to occur on the xanthan helix [18] or when xanthan is in the disordered state [19,20]. The nature of the interaction pattern as well as the amount and the position of the cross-linking site of XG remains poorly understood. To address this issue, a better understanding of the gel network is thus required.

The gel network for polymeric physical gels can be modeled as a branching process by cascade theory [21]. The branching process begins by choosing an arbitrary polymer chain as a root chain, where the conversion of a functional group creates a connection to the next chain. The connection is assumed to proceed infinitely and cyclic connectivity is not allowed in the cascade formalism. The gel network structure is thus associated with the probability of cross-linking between polymer chains in a molecular level. Recently we have extended the cascade model for single-component polymer gels to describe the gel properties of two-component polymer gels [22,23]. The interaction between the two components was assumed to follow a pair-wise reaction and it was found that the gel modulus and gel point of a mixed gel were strongly composition dependent. The model parameters, such as functionalities (number of cross-linking sites in a polymer chain) for both polymers, equilibrium constant, enthalpy of cross-linking, and entropy of cross-linking, could be obtained from experimental data using a non-linear curve fitting method. Since the synergistic interaction in the XG/LBG mixed gel can be considered to occur via the pair-wise reaction between XG and LBG, the cascade model developed for two-component polymer gels seems to be appropriate for describing its network structure.

The objective of this paper is to analyze the rheological behavior of XG/LBG mixed gels based on the cascade model developed for two-component polymer gels. The rheological behavior of XG/LBG mixed gels was examined as a function of composition, polymer concentration, and temperature. Critical gelling concentrations at different concentration ratios were also measured. The model parameters were extracted from the experimental data, and an interpretation of these parameters was then attempted in order to gain further insight into the network structure and cross-linking site of the XG/LBG mixed gel.

2. Experimental

2.1. Materials

XG and LBG were purchased from Aldrich (Milwaukee, WI) and Sigma (St. Louis, MO), respectively. The mannose/galactose ratio of LBG determined by the alditol acetate derivatives [24] is 3.3. The intrinsic viscosities obtained from an Ubbelohde capillary viscometer for XG in 0.10 M NaCl and LBG are 15.8 and 11.6 dL/g, respectively. The average molecular weights are estimated to be 0.98×10^6 and 1.69×10^6 g/mol for XG and LBG, respectively, using the Mark–Houwink equation [25,26].

2.2. Sample preparation

XG/LBG mixed gels were prepared by first dispersing appropriate amounts of XG and LBG in de-ionized water at room temperature and then heating at 85 °C for 30 min. Sodium azide of 0.05 wt% was added to prevent bacterial degradation. The hot solution was poured into the rheometer and allowed to cool to room temperature. Gels prepared from solutions with concentration ratios ($r = C_{XG}/C_{LBG}$) of 0.10, 0.33, 1.0, 3.0 and 10 were studied in the rheological measurement.

2.3. Rheological measurements

Rheological measurements were performed using a Rheometrics SR5 rheometer with a parallel plate geometry (25 mm diameter and a gap of 0.5 mm). Measurements were carried out after the sample temperature has been stabilized at 25 °C for 10 min. A strain sweep test was performed to check whether the measurements have been performed within the linear viscoelastic (LVE) regime. The storage (G') and loss (G'') moduli were recorded at 25 °C with a strain of 1% in the frequency range from 0.1 to 10 rad/s. The temperature dependence test was performed from 25 °C to 80 °C at a heating rate of 2 °C/min with the frequency held constant at 1 rad/s and the strain amplitude at 1%. Silicone grease (high vacuum grease, Dow Corning, Midland, MI) was applied around the exposed sample surface between the plates to eliminate the problem of solvent evaporation at elevated temperature. The application of grease did not affect the modulus values of the rheological measurement.

2.4. Determination of critical gelling concentrations

The melting temperature for the XG/LBG mixed gels of a series of polymer concentrations was first determined by the ''test tube upside-down'' method [27]. The test tube was immersed in a water bath, where the temperature was allowed to rise at a rate of 1 K/min approximately. Then the critical gelling concentration at a specific temperature was obtained from the interpolation of the melting temperature–concentration curve. This procedure was repeated for samples of different concentration ratios.

3. Results and discussion

3.1. Rheological properties

A strain sweep with a frequency of 1 rad/s was performed prior to the gel modulus measurement to check the linear viscoelastic regime. In the LVE regime, G' and G'' are independent of

strain amplitude. Fig. 1 shows the strain (γ) dependence of G' and G'' for XG/LBG mixed gels at different polymer concentrations. It can be seen that there is no abrupt change in G' and G'' up to a strain amplitude of 10% for the concentrations investigated. Thus the gel modulus measurement conducted at 1% strain is well within the LVE. Fig. 1 also shows that G' is approximately an order of magnitude greater than G'' for all the three samples, which is typical of a strong gel.

The gel behavior can be further demonstrated by a frequency sweep. Fig. 2 shows the frequency (ω) dependence of G' and G'' for the XG/LBG mixed gel ($r = 1$ and $C = 5$ g/L) at three different temperatures. At low temperatures, G' is far greater than G'' and exhibits a pronounced plateau over two decades of frequency, showing a typical gel behavior. At 35 °C, G' still dominates G'', but a slight drop-off in the G' and G'' plateaus toward low frequencies is observed. In the drop-off region, the frequency dependencies of G' and G'' ($G' \propto \omega^{0.6}$ and $G'' \propto \omega^{0.4}$) are weaker than those for a Maxwellian fluid ($G' \propto \omega^2$ and $G'' \propto \omega$), showing a gel-like behavior.

In our previous studies [22,23], we have demonstrated that the cascade analysis of a two-component polymer gel can be achieved by examining the concentration-dependence or temperature-dependence gel modulus data recorded at different concentration ratios. In what follows, these two types of data are presented and discussed.

Fig. 3 shows the concentration dependence of G' for XG/LBG mixed gels measured at different concentration ratios. It can be seen that the gel modulus increases with increasing polymer concentration due to an increase in the density of the cross-links formed via the interaction between XG and LBG. It is noted that the gel modulus is strongly dependent on the concentration ratio with $r = 1$ giving the highest modulus value. The values of modulus for a specific concentration ratio are somewhat comparable to those for its reciprocal r value (e.g., the modulus data for $r = 0.1$ and $r = 10$). This type of concentration ratio effect indicates that the functionalities of XG and LBG are comparable. However, the exact functionalities of XG and LBG have to be determined by fitting the data to the cascade model using a non-linear regression method (see below).

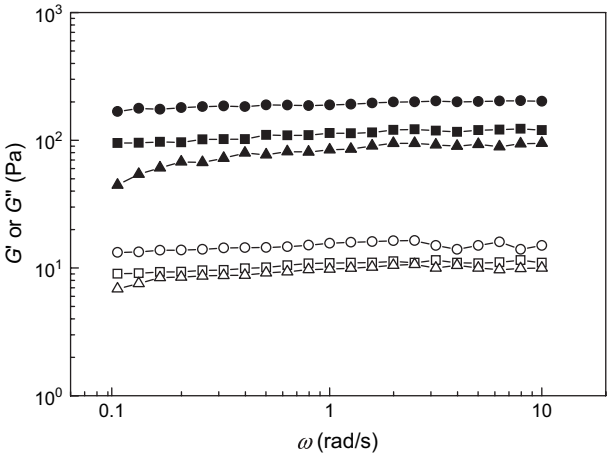

Fig. 2. Frequency sweep of XG/LBG mixed gels ($r = 1$, $C = 5$ g/L) with a strain amplitude of 1% (filled and open symbols represent G' and G'', respectively; ●/○, 25 °C; ■/□, 30 °C; ▲/△, 35 °C).

The concentration dependence of G' for physical gels can be simply approximated by a power law: $G' \propto C^n$, where n is the power-law exponent. An n value of approximately two is obtained from the plot of $\log G'$ vs. $\log C$ at different concentration ratios (Fig. 4). This value is in good agreement with that reported for one-component thermo-reversible gels [28,29]. Ross-Murphy and McEvoy have argued that the square power-law relationship is valid only when the concentration range investigated is far greater than the critical gelling concentration [30]. The power-law approximation is in fact a limiting case of the cascade model discussed below.

Fig. 5 shows the rheological meltdown data for XG/LBG mixed gels at different concentration ratios. It can be seen that increasing the temperature leads to a decrease in gel modulus, typical of a thermo-reversible gel. This trend can be simply explained by the reduction in the density of cross-links due to a decrease in the equilibrium constant for cross-link

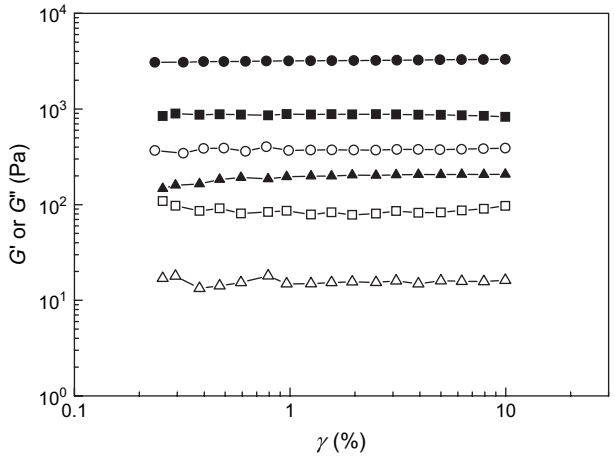

Fig. 1. Strain sweep of XG/LBG mixed gels ($r = 1$) with a frequency of 1 rad/s at 25 °C (filled and open symbols represent G' and G'', respectively; ●/○, $C = 20$ g/L; ■/□, $C = 10$ g/L; ▲/△, $C = 5$ g/L).

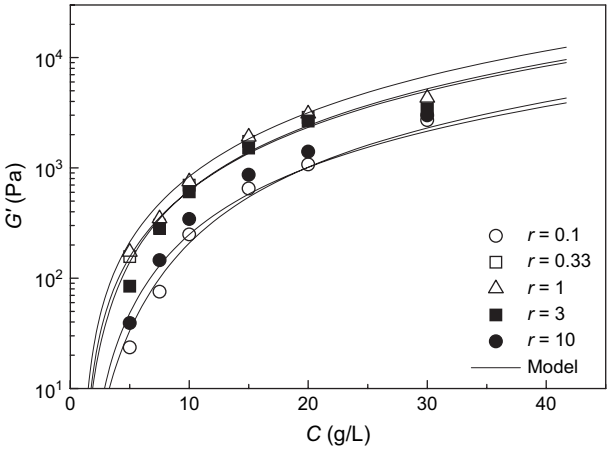

Fig. 3. Effect of concentration ratio on the concentration dependence of G' for XG/LBG mixed gels at 25 °C. The solid curves are derived by the cascade model using the parameter set $f_{LBG} = 1000$ and $f_{XG} = 100$ as given in Table 1.

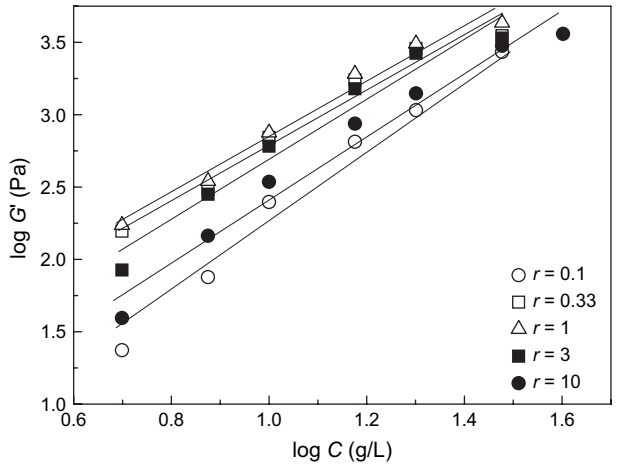

Fig. 4. Power law dependence of storage modulus as a function of concentration.

formation at elevated temperature. The melting temperature (the temperature at which $G' < G''$) for each sample cannot be observed due to the limitation of the rheometer. It is also noted that like the concentration dependence result, the gel modulus in Fig. 5 is dependent on the concentration ratio and the sample with $r = 1$ has the highest modulus value.

3.2. Cascade analysis of gel modulus data

The modulus data in Figs. 3 and 5 can be analyzed using the cascade model. In our previous paper [22], we have developed the cascade model for a two-component polymer gel by assuming that the cross-link of the gel network is formed via the interaction between the functional groups A and B of the two components:

$$A + B \leftrightarrow AB \tag{1}$$

The conversions α_A and α_B of the functional groups A and B can be determined using the stoichiometric relationship

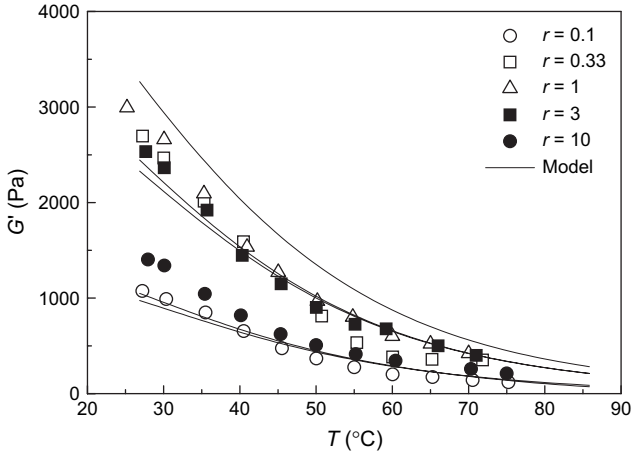

Fig. 5. Effect of concentration ratio on the temperature dependence of G' for XG/LBG mixed gels ($C = 20$ g/L). The solid curves are derived by the cascade model using the parameter set $f_{LBG} = 1000$ and $f_{XG} = 500$ as given in Table 2.

$$\left(\frac{C_A}{M_A}\right) f_A \alpha_A = \left(\frac{C_B}{M_B}\right) f_B \alpha_B \tag{2}$$

and the equilibrium expression

$$K = \frac{\alpha_A}{(C_B/M_B) f_B (1-\alpha_A)(1-\alpha_B)} \tag{3}$$

where K denotes the equilibrium constant for cross-link formation, and C, M, and f are the polymer concentration, molecular weight, and functionality, respectively.

The gel modulus is expressed in terms of the number of elastically active network chains per repeating unit N_{eA} and N_{eB}

$$G = aRT[N_{eA}(C_A/M_A) + N_{eB}(C_B/M_B)] \tag{4}$$

where a is the front factor measuring the deviation from ideal rubber behavior. The expressions for N_{eA} and N_{eB} can be written as a function of the conversions and functionalities

$$N_{eA} = \frac{1}{2} f_A \alpha_A (1 - v_B) \times [1 - v_A - (f_A - 1)\alpha_A v_A (1 - v_B)/(1 - \alpha_A + \alpha_A v_B)] \tag{5a}$$

$$N_{eB} = \frac{1}{2} f_B \alpha_B (1 - v_A) \times [1 - v_B - (f_B - 1)\alpha_B v_B (1 - v_A)/(1 - \alpha_B + \alpha_B v_A)] \tag{5b}$$

where v_A and v_B denote the extinction probabilities. At fixed conversions and functionalities, v_A and v_B can be determined numerically by the following equations

$$v_A = (1 - \alpha_A + \alpha_A v_B)^{f_A - 1} \tag{6a}$$

$$v_B = (1 - \alpha_B + \alpha_B v_A)^{f_B - 1} \tag{6b}$$

At a fixed temperature, the concentration dependence of gel modulus can be constructed using Eqs. (2)–(6). Four parameters, a, K, f_A, and f_B, are required to fit experimental G' vs. C data to Eq. (4). When the temperature varies, the temperature dependence of the equilibrium constant is assumed to follow the van't Hoff type equation [23]

$$K = \exp\left(\frac{\Delta S^\circ}{R} - \frac{\Delta H^\circ}{RT}\right) \tag{7}$$

where ΔH° and ΔS° are the enthalpy change and entropy change per cross-link. The temperature dependence of gel modulus can thus be constructed using the additional Eq. (7), and two more parameters, ΔH° and ΔS°, are required, replacing the equilibrium constant, to fit experimental G' vs. T data to Eq. (4).

To find the best-fit values of a and K for the concentration-dependent data, or a, ΔH°, and ΔS° for the temperature-dependent data, a non-linear least-squares method was

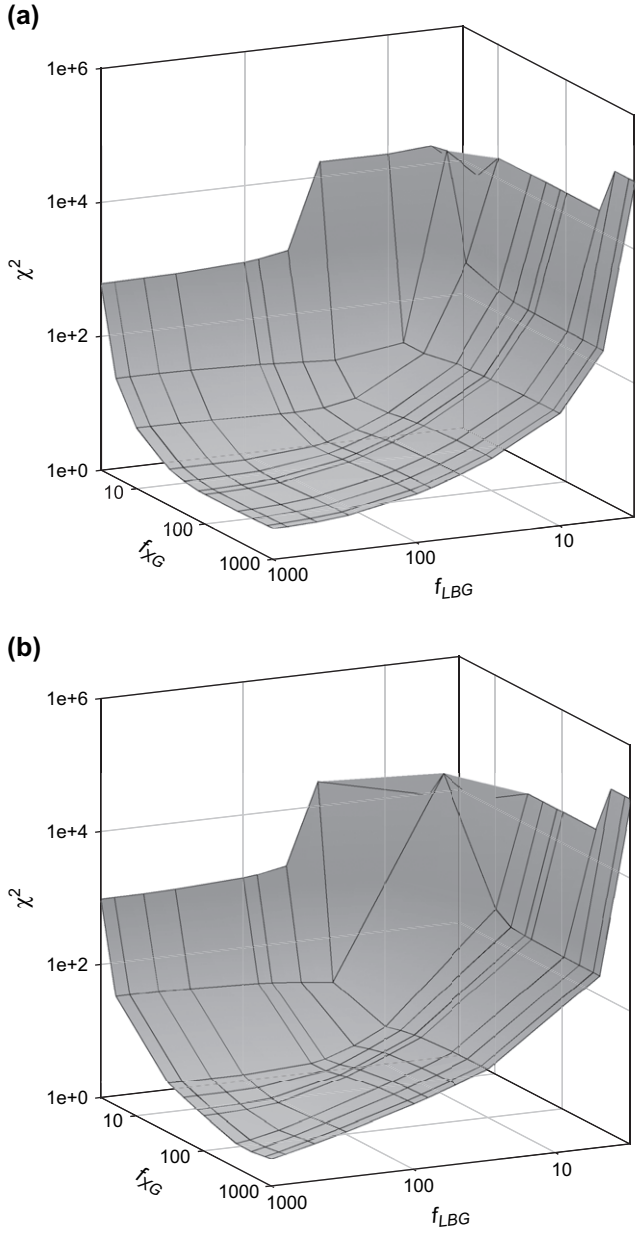

Fig. 6. The object function χ^2 as a function of component functionalities obtained by using Eq. (8). (a) Fitting the modulus-concentration dependence data. (b) Fitting the modulus-temperature dependence data.

developed using the Levenberg–Marquardt algorithm [31] to minimize an object function χ^2, which is defined as

$$\chi^2 = \sum \left(\ln G'^{\exp} - \ln G'^{\mathrm{cal}}\right)^2 \tag{8}$$

where $G'^{\exp}$ and G'^{cal} represent the experimental and calculated G' values, respectively. On the other hand, the best-fit values of f_A and f_B have to be determined using a direct search method due to their discrete nature.

Fig. 6 shows the results of fitting the modulus data in Figs. 3 and 5 to Eq. (4). The minimized object function χ^2 is plotted as a function of f_{LBG} and f_{XG}. It can be seen that χ^2 has a minimum at large f_{LBG} and f_{XG} for both sets of data. The exact values of χ^2 at some set of functionalities are listed in Tables 1 and 2. Table 1 shows that on fitting the concentration-dependent gel modulus data, though χ^2 has a minimum at $f_{XG} = 100$ and $f_{LBG} = 1000$, the χ^2 value does not vary significantly in the range of $f_{XG} = 50$–1000 and $f_{LBG} = 300$–1000. The model curves obtained using the parameter set at $f_{XG} = 100$ and $f_{LBG} = 1000$ agree well with the experimental data, as shown in Fig. 3. The result of fitting the temperature-dependent gel modulus data is somewhat different. Table 2 shows that the best-fit value of f_{LBG} is 1000, identical to that in Table 1, but for f_{XG}, χ^2 has a minimum located at $f_{XG} = 500$ rather than 100. The parameter set at $f_{XG} = 500$ and $f_{LBG} = 1000$ is then used to generate the temperature-dependent G' curves, which agree fairly with the experimental data, as shown in Fig. 5.

Table 1
Best-fit cascade parameters for the modulus-concentration data in Fig. 3 at some functionality sets

f_{LBG}	f_{XG}	a	K (L/mol)	χ^2
100	100	10.8	293	4.76
300	100	7.50	120	3.12
500	100	7.23	72.4	2.90
800	100	7.09	45.2	2.81
1000	30	12.5	87.9	3.52
1000	50	9.20	62.5	3.01
1000	80	7.56	43.5	2.82
1000	100	6.81	36.9	2.79
1000	300	5.42	14.1	2.80
1000	500	5.14	8.71	2.83
1000	800	4.90	5.62	2.87
1000	1000	4.92	4.47	2.88

Before explaining the discrepancy in the best-fit f_{XG} values, we first examine the validity of these values, which should be consistent with the chemical structure of xanthan. The repeating unit of xanthan consists of five hexoses with a molar mass of approximately 900 g/mol (estimation based on a pyruvate content of 50% and an acetate content of 50%). Since the molecular weight of the XG sample is ca. 0.98×10^6 g/mol, a value of $f_{XG} = 100$ implies that a junction zone is formed in every 10 repeating units along the xanthan backbone. In contrast, a value of $f_{XG} = 500$ corresponds to the formation of junction zones in approximately every three repeating units. Dea et al. [17] have proposed that the interaction of LBG with XG involves the LBG segment with more than six consecutive galactose-free mannose residues. The junction zone is thus composed of a galactose-free LBG segment and several XG repeating units. This model excludes the possibility of a dense arrangement of junction zones along the XG backbone. The value of $f_{XG} = 500$ thus seems to be too high to be realistic. The overestimation of f_{XG} can be attributed to the possible occurrence of a secondary process, such as a structural rearrangement, during the rheological meltdown. The temperature-induced structural rearrangement has been observed in a calorimetric thermogram for glucomannan/xanthan mixed gels [3] and our previous paper [23] has demonstrated that the presence of a structural rearrangement significantly influences the result of cascade modeling. Consequently, the result

Table 2
Best-fit cascade parameters for the modulus-temperature data in Fig. 5 at some functionality sets

f_{LBG}	f_{XG}	a	$-\Delta H^\circ$ (kJ/mol)	$-\Delta S^\circ$ (J/K mol)	χ^2
80	500	5.01	36.1	77.0	12.6
100	500	4.19	37.2	81.3	10.7
300	500	1.77	43.5	104	5.26
500	500	1.17	47.3	117	3.86
800	500	0.86	49.8	126	2.96
1000	80	2.61	41.9	96.0	4.25
1000	100	2.16	43.3	101	3.90
1000	300	0.93	50.6	126	2.71
1000	500	0.76	50.6	129	2.67
1000	800	0.77	48.2	126	2.87
1000	1000	0.79	46.8	124	2.97

obtained from fitting the concentration-dependent gel modulus data seems to be more reliable.

The f_{LBG} value also has to be consistent with the chemical structure of LBG. LBG is a galactomannan consisting of a mannan backbone randomly branched with single galactose units. The cross-linking site of LBG with XG is composed of consecutive unsubstituted mannose residues. This has been demonstrated by the fact that the galactose-depleted guar gum is capable of forming a synergistic gel with XG similar to LBG [32], which is not possible for guar gum due to its lack of consecutive unsubstituted mannan segments. The distribution of unsubstituted mannan segments in an LBG chain can be calculated using McCleary et al.'s theoretical prediction [33]. Fig. 7 shows the distribution profile of the unsubstituted mannan segments of size m and the accumulated profile for segment sizes larger than $m-1$ for the LBG sample. The accumulated value roughly represents the functionality of LBG. Using this approximation, the values of $f_{LBG}=1000$ and 300 correspond to the numbers of segment sizes with more than three and six consecutive unsubstituted mannose residues, respectively. The value of $f_{LBG}=300$ is consistent with Dea et al.'s report [17]. However, the cascade analysis suggests that the best-fit value of f_{LBG} is greater than 300, which implies

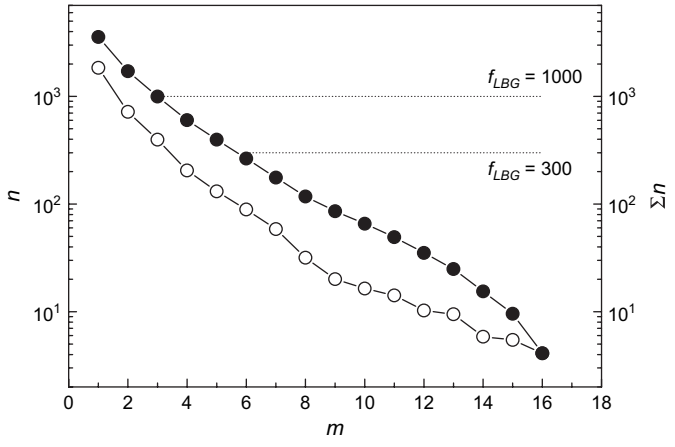

Fig. 7. Distribution of unsubstituted mannose segments in an LBG chain (m: segment size; n: number of unsubstituted mannose segments (○); Σn: accumulated value of n for segment size larger than $m-1$ (●)). Estimation is made based on the theoretical distribution function in Ref. [33].

that it is likely that the segment with less than six consecutive unsubstituted mannose residues also participates in the formation of junction zones.

Tables 1 and 2 also show the values of other cascade parameters, including a, ΔH°, and ΔS°. It can be seen that the values of the front factor in Table 1 are all greater than unity, indicating that the elastically active network chains are stiffer than those in an ideal rubber network. The greater-than-unity a values also imply that there is a significant enthalpic contribution to the gel elasticity. An interesting observation when comparing the values in the literature is that the best-fit a value at $f_{LBG}=1000$ is intermediate between values for LBG gels [34] ($a=1.12$ and 2.20 at $f_{LBG}=1000$) and agarose gels [35] ($a=57$ at $f_{agarose}=25$). Since the network chain of XG/LBG mixed gels is composed of XG and LBG, the a value must reflect a combination of both types of chains. XG, which is capable of forming helices, may have a chain stiffness comparable to that of agarose gels, which are composed of bundles of agarose helices. On the other hand, the LBG network chain in XG/LBG mixed gels should be identical to that in LBG gels. Therefore, it is reasonable to find that the chain stiffness for XG/LBG mixed gels lies intermediate between these two biopolymer gels.

The a values obtained from the modulus-temperature data (Table 2), in contrast, are close to unity. Since we have argued that the rheological meltdown may involve a structural rearrangement, the resulting a values may be misleading. Nevertheless, the ΔH° and ΔS° values can serve as thermodynamic parameters for characterizing the rheological meltdown process. The $-\Delta H^\circ$ and $-\Delta S^\circ$ values in Table 2 are significantly lower than those obtained from the meltdown of LBG gels [34] ($-\Delta H^\circ=99.6$ kJ/mol and $-\Delta S^\circ=201$ J/K mol). Due to the uncertainties of the melting process, an interpretation of the interaction between segments of XG and LBG based on these values is not possible and only a qualitative statement can be made concerning the cross-links. The negative sign of ΔS° demonstrates that there is an entropy loss when the cross-links between segments of XG and LBG are formed, which is consistent with the enthalpy–entropy compensation phenomenon [36] often observed for weak interactions.

3.3. Critical gelling concentrations

Fig. 8 shows the dependence of critical gelling concentration on composition at different temperatures. Due to a decrease in the equilibrium constant for the association reaction (Eq. (1)) at elevated temperatures, higher polymer concentrations are required for gelation; thus the critical gelling concentration increases with increasing temperature. It is noted that the critical gelling concentration–composition data has a minimum at $r=0.33$, rather than unity. The unsymmetry of the plot implies unequal values for f_{XG} and f_{LBG}, as suggested by our previous work [22]. It is also noted that the samples of $r=100$ behave similarly to pure xanthan solutions, indicating that the gelling behavior at $r=100$ is determined by the self-association of xanthan. It is evident that the self-association of xanthan becomes significant at high r values. Since the self-association

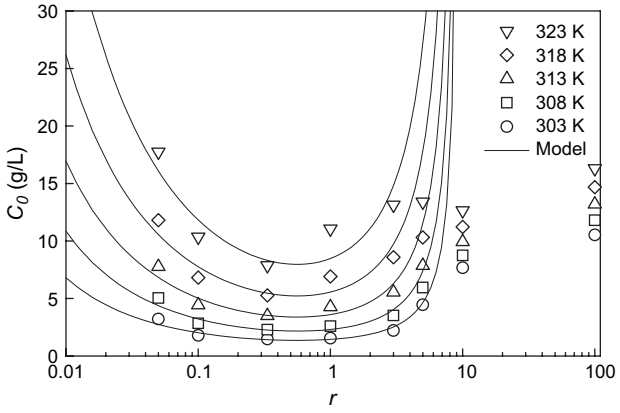

Fig. 8. Composition dependence of the critical gelling concentration for XG/LBG mixed gels at different temperatures.

is not treated in the current model, the cascade analysis of the critical concentration data uses only data at low r values.

In the cascade model, the critical gelling concentration C_0 for a two-component polymer gel at a fixed composition is determined by the equilibrium constant and functionalities [22]

$$C_0 = \frac{(1+r)\alpha_{A0}M_B}{rKf_B(1-\alpha_{A0})(1-\alpha_{B0})} \tag{9}$$

where α_{A0} and α_{B0} are the critical conversions for the functional groups A and B, respectively. The critical conversions are also written as functions of f_A and f_B

$$\alpha_{A0} = \left(\frac{rf_BM_A}{f_AM_B}\right)^{1/2}[(f_A-1)(f_B-1)]^{-1/2} \tag{10a}$$

$$\alpha_{B0} = \left(\frac{rf_BM_A}{f_AM_B}\right)^{-1/2}[(f_A-1)(f_B-1)]^{-1/2} \tag{10b}$$

The C_0 vs. r data in Fig. 8 can be fitted to Eqs. (9) and (10) by adjusting the parameters K, f_{XG}, and f_{LBG}. This was achieved by minimizing an object function χ^2 with respect to K for a specific set of f_{XG} and f_{LBG}. The object function includes data at various temperatures and is defined as follows:

$$\chi^2 = \sum\left(\ln C_0^{exp} - \ln C_0^{cal}\right)^2 \tag{11}$$

The set of f_{XG} and f_{LBG} having a minimum χ^2 value is determined as the best-fit parameter set. The K values obtained using the best-fit set of f_{XG} and f_{LBG} are then expressed as a function of temperature.

Fig. 9 shows the results of fitting the critical gelling concentration data using Eqs. (10) and (11). Only data points with $r \leq 3$ in Fig. 8 were used in order to eliminate the effect of the self-association of xanthan. The lowest χ^2 value occurs at $f_{XG} = 30$ and $f_{LBG} = 5$. The model curves generated using this parameter set are in good agreement with the experimental data for $r \leq 3$, as shown in Fig. 8. It is noted that the best-fit functionality values are far less than those obtained from the modulus data. This discrepancy is possibly due to the fact that the gel networks probed by the critical gelling concentration measurement and by the shear rheometer are not the same.

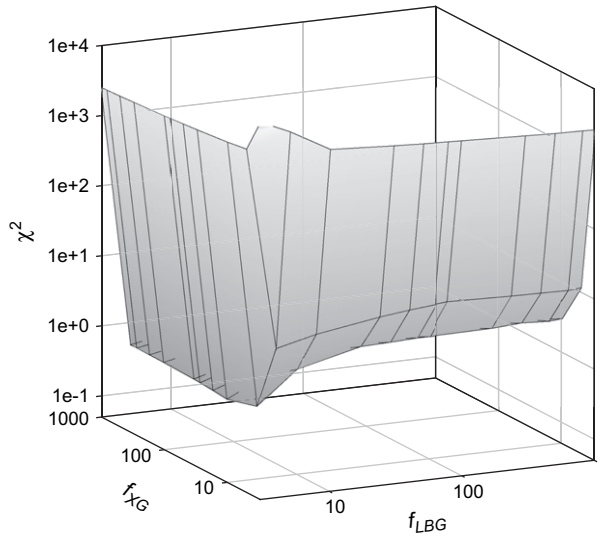

Fig. 9. The object function χ^2 as a function of component functionalities obtained by using Eq. (11).

The former tests the ability of a gel to support its own weight under gravity, whereas the latter measures the ability of a gel to restore its original dimensions. The value of $f_{XG} = 30$ implies that a junction zone is formed in every 36 repeating units along the XG backbone, and the value of $f_{LBG} = 5$ suggests that the cross-linking site of LBG involves the LBG segment with more than 15 unsubstituted mannose residues (as suggested by Fig. 7). It seems that the interaction between short segments of XG and LBG cannot be detected by the critical gelling concentration measurement and this explains the low best-fit values for f_{XG} and f_{LBG}.

The equilibrium constant obtained from the fit decreases with increasing temperature. Fig. 10 shows the van't Hoff

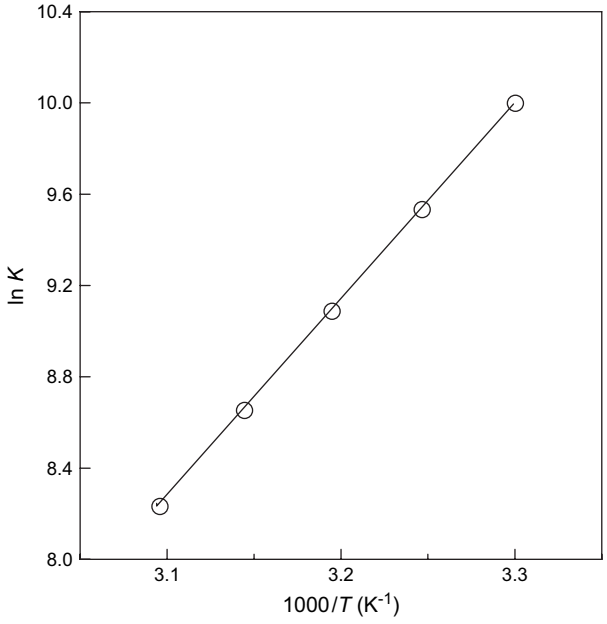

Fig. 10. Van't Hoff plot of the equilibrium constant obtained from the cascade analysis of the critical concentration data.

plot of the equilibrium constants at $f_{XG} = 30$ and $f_{LBG} = 5$. The linearity of the plot indicates that the data obey the van't Hoff type equation (Eq. (7)). The resulting ΔH° and ΔS° values are -71 kJ/mol and -151 J/K mol, respectively. The ΔH° value is consistent with those obtained from the Ferry–Eldridge plot [23] (-67 to -87 kJ/mol), but somewhat larger than those extracted from the G' vs. T data. It is also interesting to note that the dimensionless enthalpy–entropy ratio $\Delta H^\circ/300\Delta S^\circ$ has a value of 1.57, which is almost identical to the value reported for the associations of low-molecular-weight molecules in solution [36]. This equivalence suggests that the cross-link formed between segments of LBG and XG occurs in a manner similar to the associations of small molecules.

4. Conclusions

The elastic properties and critical gelling behavior of XG/LBG mixed gels were analyzed using a two-component cascade model, which assumed that the gel network is developed simply via the cross-links between segments of LBG and XG. The mixed gel network in the model was represented by a branching tree, where the junctions were determined by the probability of cross-links between XG and LBG. The model parameters estimated by fitting the experimental data with the model thus provided some information about the interaction pattern of cross-links as well as the rigidity of network chains.

The analysis result shows that the G' vs. C and G' vs. T data can be successfully approximated by the model, whereas the model is only valid for the C_0 vs. r data at low r values. The failure in modeling the data at high r values is due to that the effect of the self-association of xanthan becomes significant when XG is in excess amounts. The best-fit f_{XG} and f_{LBG} values obtained from the G' vs. C data were found to be 100 and 1000, respectively. The f_{LBG} value implies that cross-links are formed via the interaction of XG with LBG segments of more than three consecutive unsubstituted mannose residues. The greater-than-unity value of the front factor also reflects the presence of an enthalpic contribution to the gel elasticity. The cascade analysis of the G' vs. T data, on the other hand, leads to an unrealistically high f_{XG} value. The anomaly is possibly due to the existence of a secondary mechanism other than the dissociation of cross-links during the rheological meltdown process. The cascade analysis of the C_0 vs. r data results in smaller functionality values ($f_{XG} = 30$ and $f_{LBG} = 5$) with $\Delta H^\circ = -71$ kJ/mol and $\Delta S^\circ = -151$ J/K mol. The differences in the best-fit f_{XG} and f_{LBG} values obtained from the modulus data and the critical gelling concentration data can be explained by the fact that the gel network probed by the two approaches is not the same. The gel network probed by the "test tube upside-down" method possibly involves only the cross-links between long segments of XG and LBG, thus giving smaller functionalities.

References

[1] Dea ICM, Morris ER, Rees DA, Welsh EJ, Barnes HA, Price J. Carbohydr Res 1977;57:249.
[2] Lundin L, Hermansson AM. Carbohydr Polym 1994;26:129.
[3] Goycoolea FM, Richardson RK, Morris ER, Gidley MJ. Macromolecules 1995;28:8308.
[4] Copetti G, Grassi M, Lapasin R, Pricl S. Glycoconjugate J 1997;14:951.
[5] Schorsch C, Garnier C, Doublier JL. Carbohydr Polym 1997;34:165.
[6] Jansson PE, Kenne L, Lindverg B. Carbohydr Res 1975;45:275.
[7] Melton LD, Mindt L, Rees DA, Sanderson GR. Carbohydr Res 1976;46:245.
[8] Sato T, Norisuye T, Fujita H. Polym J 1984;16:341.
[9] Berth G, Dautzenberg H, Christensen BE, Harding SE, Rother G, Smidsrød O. Macromolecules 1996;29:3491.
[10] Milas M, Rinaudo M. Carbohydr Res 1979;76:189.
[11] Milas M, Rinaudo M. Carbohydr Res 1986;158:191.
[12] Smith IH, Symes KC, Lawson CJ, Morris ER. Int J Biol Macromol 1981;3:129.
[13] Rodd AB, Dunstan DE, Boger DV. Carbohydr Polym 2000;42:159.
[14] Dea ICM, Morrison A. Adv Carbohydr Chem Biochem 1975;31:241.
[15] Garcia-Ochoa F, Casas JA. J Sci Food Agric 1992;59:97.
[16] Mao CF, Chen JC. Food Hydrocolloids 2006;20:730.
[17] Dea ICM, Clark AH, McCleary BV. Carbohydr Res 1986;147:275.
[18] Morris ER, Rees DA, Young G, Walkinshaw MD, Darke AJ. Mol Biol 1977;110:1.
[19] Cairns P, Miles MJ, Morris VJ. Nature 1986;322:89.
[20] Cairns P, Miles MJ, Morris VJ, Brownsey GJ. Carbohydr Res 1987;160:411.
[21] Dobson GR, Gordon M. J Chem Phys 1965;43:705.
[22] Mao CF, Chen JC. J Appl Polym Sci 2006;99:2771.
[23] Mao CF. J Appl Polym Sci, in press.
[24] Blakeney AB, Harris PJ, Henry RJ, Stone BA. Carbohydr Res 1983;113:291.
[25] Gaisford SE, Harding SE, Mitchell JR, Bradley TD. Carbohydr Polym 1986;6:423.
[26] Capron I, Brigand G, Muller G. Polymer 1997;38:5289.
[27] Hong PD, Chen JH. Polymer 1998;39:711.
[28] Ferry JD. J Am Chem Soc 1948;70:2244.
[29] Koltisko B, Keller A, Litt M, Baer E, Hiltner A. Macromolecules 1986;19:1207.
[30] Ross-Murphy SB, McEvoy H. Br Polym J 1986;18:2.
[31] Marquardt DW. J Soc Ind Appl Math 1963;11:431.
[32] Pai VB, Khan SA. Carbohydr Polym 2002;49:207.
[33] McCleary BV, Clark AH, Dea ICM, Rees DA. Carbohydr Res 1985;139:237.
[34] Richardson PH, Clark AH, Russell AL, Aymard P, Norton IT. Macromolecules 1999;32:1519.
[35] Watase M, Nishinari K, Clark AH, Ross-Murphy SB. Macromolecules 1989;22:1196.
[36] Searle MS, Westwell MS, Williams DH. J Chem Soc Perkin Trans 1995;2:141.